Photochemistry and Photobiology, 2004, 79(3): 272–279

# A Far-red Fluorescent Contrast Agent to Image Epidermal Growth Factor Receptor Expression

**Elizabeth R. Hsu[1], Eric V. Anslyn[2], Su Dharmawardhane[3], Reza Alizadeh-Naderi[4], Jesse S. Aaron[1], Konstantin V. Sokolov[5], Adel K. El-Naggar[6], Ann M. Gillenwater[4] and Rebecca R. Richards-Kortum*[1]**

[1]Department of Biomedical Engineering, The University of Texas at Austin, Austin, TX;
[2]Department of Chemistry and Biochemistry, The University of Texas at Austin, Austin, TX;
[3]Section of Molecular Cell and Developmental Biology, The University of Texas at Austin, Austin, TX;
[4]Department of Head and Neck Surgery, The University of Texas M.D. Anderson Cancer Center, Houston, TX;
[5]Department of Imaging Physics, The University of Texas M.D. Anderson Cancer Center, Houston, TX and
[6]Department of Pathology, The University of Texas M.D. Anderson Cancer Center, Houston, TX

**Received 3 September 2003; accepted 6 January 2004**

## ABSTRACT

**Recent developments in optical technologies have the potential to improve the speed and accuracy of screening and diagnosis of curable precancerous lesions and early cancer, thereby decreasing the costs of detection and management of epithelial malignancies. The development of molecular-specific contrast agents for markers of early neoplastic transformation could improve the detection and molecular characterization of premalignant lesions. In the oral cavity, epidermal growth factor receptor (EGFR) overexpression has been identified in early stages of premalignant lesions of the oral squamous cell carcinoma; therefore, real-time assessment of EGFR expression could serve as a biomarker for oral neoplasia. The purpose of our study was to develop a molecular-specific optical contrast agent targeted against EGFR for *in vivo* assessment of epithelial neoplasia using a monoclonal antibody and the far-red fluorescent dye, Alexa Fluor® 660 streptavidin. In addition to demonstrating the specificity of the contrast agent for EGFR in cell lines, we document the ability to achieve penetration through 500 μm thick epithelial layers using multilayer tissue constructs and permeability-enhancing agents. Finally, using the fluorescence intensity of the contrast agent on fresh oral cavity tissue sections, we were able to distinguish abnormal from normal oral tissue. This contrast agent should have important clinical applications for use in conjunction with fluorescence spectroscopy or imaging (or both) to facilitate tumor detection and demarcation.**

*To whom correspondence should be addressed at: Department of Biomedical Engineering, The University of Texas at Austin, 1 University Station C0803, Austin, TX 78712, USA. Fax: 512-475-8854; e-mail: kortum@mail.utexas.edu

*Abbreviations:* BSA, bovine serum albumin; CDC, Centers for Disease Control and Prevention; DMEM, Dulbecco's modified essential media; DIC, differential interference contrast; DMSO, dimethyl sulfoxide; EABA, endogenous avidin-binding activity; EGF, epidermal growth factor; EGFR, epidermal growth factor receptor; FBS, fetal bovine serum; FDA, Food and Drug Administration; H&E, hematoxylin and eosin; i.v., intravenous; NIH, National Institutes of Health; NSF, National Science Foundation; PBS, phosphate-buffered saline; PVP, polyvinylpyrrolidone; SCC, squamous cell carcinoma; SNR, signal-to-noise ratio.



## INTRODUCTION

Advances in optical technologies that offer novel noninvasive tools to improve the screening and diagnosis of cancer and its precursors have recently generated much excitement. These methods have the potential to provide diagnostic information in near real-time without the need for biopsy and with minimal patient discomfort and cost. Numerous optical techniques have been developed and tested *in vivo* in pilot studies, including multispectral fluorescence imaging (1,2), multispectral reflectance imaging with polarized and unpolarized light (2,3), confocal microscopy (4,5), reflectance spectroscopy with polarized and unpolarized light (6–8) and fluorescence spectroscopy (7,9–11).

The oral cavity is an ideal site for the application of optical techniques because of accessibility and convenient visualization. Currently, diagnosis of oral cancer is achieved through visual identification and recognition, which relies on the experience of the treating clinician. Optical techniques could potentially improve diagnosis and detection of oral cancer by allowing objective assessment of the molecular and biochemical changes in neoplastic tissue relative to normal tissue. Successful application and validation of these techniques will lead to better screening and early detection of premalignant lesions, reducing incidence of cancer in high-risk individuals.

Recently, *in vivo* studies have demonstrated the ability of fluorescence spectroscopy to distinguish neoplasia in the oral cavity based on autofluorescence. Excitation wavelengths optimal for diagnosis of invasive carcinoma, early carcinoma, and dysplasia lie within the range of 300–440 nm (10,12–16). Although preliminary results with autofluorescence are promising, there are several limitations. First, autofluorescence signals tend to be relatively weak, photobleach rapidly, and are subject to low signal-to-noise ratio (SNR). Second, the penetration depth of the near-UV and blue excitation wavelengths is relatively limited, implying that deeper lesions or deeper margins of superficial tumors cannot be easily evaluated.

Molecular-specific, exogenous, optically active contrast agents that bind to biomarkers modified early during neoplastic transformation may facilitate the detection of early neoplastic lesions (17) and improve diagnostic accuracy and contrast. The use of a highly stable, high–quantum yield fluorophore conjugated to

a molecular-specific probe of the biomarker would also allow increased SNR compared with autofluorescence. In addition, use of an exogenous fluorophore with excitation and emission wavelengths in the red to near-infrared region increases the penetration depth.

Several studies have shown overexpression of epidermal growth factor receptor (EGFR) in premalignant and invasive oral squamous epithelial lesions. EGFR expression is detected at all stages of carcinogenesis, from normal-early hyperplasia, dysplasia to invasive carcinoma (18,19). EGFR expression is elevated during the progression from hyperplasia to dysplasia and increases during progression from dysplasia to invasive squamous cell carcinoma (SCC) (20). Moreover, EGFR expression is elevated in normal epithelium that is adjacent to tumor (20), regardless of tobacco and alcohol abuse (21). Nouri *et al*. (22) found that 73% of the invasive oral SCC they studied showed strong expression of EGFR. Other reports have estimated overexpression of EGFR in all oral cancers at 50–98% (23).

Soukos *et al*. (24) targeted SCC by conjugating an EGFR antibody to a photoactive molecule and demonstrated regression of premalignant lesions in the Syrian golden hamster cheek model after intravenous (i.v.) injection of the conjugate and exposure to therapeutic doses of light. In addition, they were able to visualize dysplasia in their model using a conjugate of the antibody and a fluorescent dye 3 days after i.v. injection of the antibody–dye conjugate. However, for diagnostic purposes, topical application of the contrast agent would be preferable to minimize patient discomfort, systemic exposure to the contrast agent and possible immunogenic effects.

The purpose of this study was to develop and evaluate a molecular-specific contrast agent to EGFR using a monoclonal antibody and far-red fluorescent dye that could be applied topically for detection of oral cavity neoplasia in humans. The first step in the development of a contrast agent for potential use in *in vivo* detection of oral cancer is to test the efficacy of the contrast agent in *in vitro* and *ex vivo* models. In this study, we demonstrate the specificity of the agent for imaging EGFR in cancer cell lines and the ability to penetrate throughout 500 μm thick multilayer epithelial tissue constructs when applied topically with permeability-enhancing agents such as dimethyl sulfoxide (DMSO), polyvinylpyrrolidone (PVP) and bovine serum albumin (BSA). To test the penetration depth of the contrast agents across multiple layers of epithelial cells, multilayer tissue constructs that have been shown to mimic the optical properties of the epithelial layer *in vivo* were used (25). Finally, we demonstrate the potential use of the fluorescence intensity of the contrast agent to distinguish abnormal tissue from normal tissue using fresh tissue slices prepared from biopsy samples from the oral cavity. We conclude that this contrast agent could potentially be used in conjunction with fluorescence spectroscopy or imaging (or both) to improve quantitative, objective tumor detection and demarcation.

## MATERIALS AND METHODS

*Contrast agent.* The antibody used in the contrast agent was a biotinylated mouse monoclonal anti-human EGFR (clone 111.6, 200 μg/mL, LabVision NeoMarkers, Fremont, CA) and was used at a 1:10 dilution. The antibody is targeted against the extracellular domain of EGFR and blocks the binding of epidermal growth factor (EGF) to the receptor. Alexa Fluor® 660 streptavidin (Molecular Probes, Eugene, OR) was used as the far-red fluorescent marker. Alexa Fluor® 660 streptavidin has a broad absorption peak with a maximum at 669 nm but can also be excited at 633 or 647 nm. Its emission maximum is at 690 nm, with a relative quantum yield of 0.88 compared with 7-hydroxy-9H-(1,3-dichloro-9,9-dimethylacridin-2-one). Alexa Fluor® 660 streptavidin has a degree of labeling of 4.7 moles of dye per mole of protein using an ε of 110 000 $cm^{-1}$ $M^{-1}$ at the absorbance maximum (all information on Alexa Fluor® 660 streptavidin as reported by Molecular Probes in the Certificate of Analysis for lot #65C1). The dye was provided as a 1 mg lyophilized powder and reconstituted in 1 mL of deionized water and stored in frozen aliquots. For use in labeling, it was diluted to 250 μg/mL in phosphate-buffered saline (PBS) and used at a 1:8 dilution.

*Cell lines.* Four human epithelial cell lines were used: MDA-MB-468 (American Type Culture Collection, Manassas, VA), an adenocarcinoma of the mammary gland known to overexpress EGFR at $\sim 1 \times 10^6$ receptors/cell (receptor number/cell from American Type Culture Collection and Anido *et al*. [26]); MDA-MB-435S (American Type Culture Collection), a ductal adenocarcinoma of the breast that expresses no EGFR (26); SiHa (American Type Culture Collection), a SCC of the cervix; and SqCC/Y1 (kindly provided by Reuben Lotan, at the University of Texas M.D. Anderson Cancer Center), a SCC of the buccal mucosa. MDA-MB-468 and MDA-MB-435S cells were grown in minimal essential media (Invitrogen, Carlsbad, CA) with 10% fetal bovine serum (FBS) (Hyclone, Logan, UT), penicillin, streptomycin, glutamine, sodium pyruvate, nonessential amino acids and vitamins (Invitrogen). SiHa and SqCC/Y1 cells were grown in Dulbecco's modified essential media (DMEM)–F12 (Invitrogen) with 5% FBS, penicillin, streptomycin and glutamine. To grow monolayers of cells for imaging, small wells were created using adhesive CoverWell imaging chambers (Grace Bio-Labs, Bend, OR) with a 25 mm diameter and 0.5 mm depth secured to a No. 1 24 × 40 mm glass coverslip. Cells were plated at a density of 0.2 million cells/mL in the chambers and allowed to grow for 3–4 days in a 37°C incubator with 5% $CO_2$ until 60–90% confluence.

*Multilayer tissue constructs.* Multilayer tissue constructs representing the structure of oral dysplasia were prepared using SqCC/Y1 cells. A collagen solution was prepared by combining collagen (Roche Applied Science, Indianapolis, IN) reconstituted in 0.2% sterile acetic acid, 0.2 *M* 4-(2-hydroxyethyl)-1-piperazine ethane sulfonic acid, 10× PBS and 1× PBS, final pH 7.4. SqCC/Y1 cells were resuspended in the collagen solution at a density of 80 million cells/mL. Tissue constructs were prepared by pipetting 400 μL of the cell–collagen solution into Costar Transwell inserts (VWR, West Chester, PA), 6.5 mm diameter with an 8 μm pore size, allowing the tissue constructs to gel, and adding media in the insert on top of the tissue construct and to the bottom well. PBS was added to empty wells to increase humidity within the plate. The tissue constructs were allowed to grow for 14–21 h in a 37°C incubator with 5% $CO_2$.

*Cell monolayer labeling.* Three samples were prepared: cells labeled for EGFR using the biotinylated EGFR antibody and two sets of control cells, one labeled using a biotinylated anti-human IgG (goat monoclonal, Vector Laboratories, Burlingame, CA) and another not exposed to any antibody but labeled with the Alexa Fluor® 660 streptavidin dye only. Between all changes of solution, cells were washed twice with 1× PBS. The media were removed from the wells, and cells were blocked for endogenous biotin using an Avidin/Biotin blocking kit (Vector Laboratories). Cells were successively incubated with the primary EGFR or IgG antibody and the Alexa Fluor® 660 streptavidin for 1 h at room temperature. After the final washes, PBS was added to the chambers and sealed using a microscopic slide.

*Multilayer tissue constructs labeling.* Multilayer tissue constructs were labeled in a similar fashion to the cells with either the EGFR antibody or anti-human IgG antibody. In addition, the blocking agents, antibodies and dye were added in permeability-enhancing solutions of 5% DMSO, 10% PVP or 4% BSA in addition to a PBS control. After labeling in the Transwells, the tissue constructs were removed, embedded in 3% agarose and sliced transversely into 250 μm sections using a Krumdieck tissue slicer (MD 1000-A1, Alabama Research and Development, Munford, AL), which is designed to cut fresh tissue with minimal damage. Three replicates of each experiment were performed.

*Fresh tissue slices.* Paired, clinically abnormal and clinically normal biopsies were obtained from consenting patients at the University of Texas M.D. Anderson Cancer Center. The clinical protocols were approved by the Institutional Review Boards at the University of Texas M.D. Anderson Cancer Center and the University of Texas at Austin. Biopsies were immediately placed and remained in chilled culture media until they were sectioned into 200 μm transverse slices using a Krumdieck tissue slicer. After slicing, biopsies were labeled as above. The avidin and biotin blocking solutions were added in a 5% BSA solution in PBS. A biotinylated normal mouse IgG (Vector Laboratories) was used as a control.

Hematoxylin and eosin (H&E)–stained sections were obtained for each biopsy and the slices that were labeled for EGFR and imaged.

*Imaging*. Optically sectioned fluorescence images of the samples were obtained using an inverted Lecia TCS 4D laser scanning confocal microscope, equipped with a Kr–Ar laser providing excitation at 647 nm and a 665 nm long-pass filter. Images were acquired with a 10× objective with a numerical aperture of 0.3 and working distance of 11 000 μm or 40× oil-immersion objective with a numerical aperture of 1.0 and working distance of 80 μm. The laser power for image acquisition varied between 3 and 30 μW. Stacks of images were obtained, with a z-step of 1.5–3 μm and 5–30 images per stack. The contrast, brightness, line averaging, integration time and pinhole size remained constant for all images in a single experiment.

*Image analysis*. To correct for fluctuations in laser power between image acquisitions, images were processed after collection by dividing by the laser power at the time of acquisition and then multiplying by a constant factor, which was the same for all images obtained from a single experiment. Image processing was performed using ImageJ (National Institutes of Health [NIH]). For the images of the fresh tissue slices, the mean fluorescence intensity of an image of the epithelial layer was determined by outlining the epithelial layer as a region of interest in ImageJ.

*Fluorometry*. Fluorometry was used to determine the efficacy of binding using various primary antibody concentrations, incubation times and the specificity of binding of the contrast agent. Fluorescence emission spectra of suspensions of SqCC/Y1 cells labeled for EGFR were measured in a Spex Fluorolog (JY Horiba, Edison, NJ). Approximately 8–9 million cells were harvested for each sample and resuspended in phenol red–free DMEM with 5% FBS, penicillin, streptomycin and glutamine. Labeling was performed as for cell monolayers, with the cells centrifuged at 1000 rpm for 3 min to change solutions and wash. After labeling, the cells were washed in PBS and resuspended in 3 mL of PBS for the emission scans. Fluorescence emission spectra were measured at an excitation wavelength of 633 nm and emission wavelengths from 643 to 700 nm at 5 nm increments with a 1 s integration time. Background fluorescence emission spectra were determined by pelleting the cells and measuring the supernatants of the cell suspensions. PBS was also measured as a background. The fluorescence intensity was determined by calculating the area under the emission curve after subtracting the background PBS or supernatant (or both).

To test the efficacy of labeling at various antibody concentrations and incubation times, cells were labeled using various dilutions of biotinylated EGFR antibody and biotinylated normal mouse IgG of 1:4, 1:10, 1:50 and 1:100 with a 60 min incubation time and using various incubation times of 5, 15, 30 and 60 min with a 1:10 antibody dilution.

The specificity of the contrast agent for EGFR was tested in a competitive binding study with EGF. Lyophilized EGF (Sigma Aldrich, St. Louis, MO) was reconstituted in 0.2 μm filtered 10 m*M* acetic acid with 0.1% BSA. Cells were labeled as above, with no, 0.0133, 0.133, or 1.33 μ*M* EGF added in addition to the anti-EGFR antibody.

*Quantitative flow cytometry*. Quantitative flow cytometry was performed on the SqCC/Y1 cells to determine how many receptors per cell were being labeled. Standard beads from a QIFI kit (Dako Cytomation, Carpinteria, CA) with known amounts of mouse monoclonal anti-CD5 immobilized on the surface produced a calibration curve from which the number of labeled receptors on the cells could be interpolated. Cells were harvested at 70% confluence or less and resuspended at a concentration of 1 million cells/mL in 1 mL of PBS with 5% BSA. Cells were labeled for EGFR using the unbiotinylated version of the same EGFR antibody used in the contrast agent at a 1:10 dilution in phenol red–free DMEM with 5% FBS, penicillin, streptomycin and glutamine for 1 h at room temperature with constant shaking. A secondary antibody of goat anti-mouse $F(ab')_2$-fluorescein isothiocyanate (Dako Cytomation) at a concentration of 1 mg/mL was added at a 1:10 dilution to detect the EGFR antibody. Three control samples were also prepared: cells labeled with normal mouse IgG (Vector Laboratories), cells labeled with the secondary antibody only, and unlabeled cells. MDA-MB-468 cells were also labeled for EGFR as a positive control. Quantitative flow cytometry was performed on a Coulter EPICS Elite flow cytometer with a 15 mW argon laser source at 488 nm.

*Cytotoxicity*. The cytotoxicity of Alexa Fluor® 660 streptavidin was tested by incubating SqCC/Y1 cells with 1:10, 1:20 and 1:50 dilutions of the dye and no dye. A single plate of SqCC/Y1 cells was harvested, a viability count performed and the plate split into eight plates and allowed to set for 2 days. The media were then removed and replaced with media containing the appropriate dilution of dye for a total volume of 10 mL. Two plates of each sample were prepared. After 2 days, each plate was harvested and a viability count performed.

## RESULTS

To determine the efficacy of using a molecular-specific far-red fluorescent contrast agent to EGFR to detect oral cavity neoplasia, we labeled unfixed monolayers of malignant cells, multilayer tissue constructs and fresh tissue sections from oral cavity biopsies.

### Detection of EGFR in single-cell monolayers

Fluorescence images of SqCC/Y1 cells labeled with biotinylated anti-EGFR conjugated to Alexa Fluor® 660 streptavidin obtained with a 40× objective are shown in Fig. 1 along with images of appropriate controls and images of MDA-MB-435S cells. Clear fluorescence is seen for SqCC/Y1 cells labeled with the anti-EGFR in Fig. 1a with the corresponding transmitted differential interference contrast (DIC) image in Fig. 1b. No fluorescence is seen with either the anti-IgG (Fig. 1c,d) or dye-only control (Fig. 1e,f). Similar results are seen for MDA-MB-468 and SiHa cells, with the MDA-MB-468 cells showing a much greater fluorescence intensity than the SqCC/Y1 cells (images not shown). MDA-MB-435S cells, which do not express EGFR, show very little fluorescence when labeled with the anti-EGFR (Fig. 1g).

### Detection of EGFR in multilayer tissue constructs

Fluorescence images of SqCC/Y1 tissue constructs obtained with a 10× objective are shown in Fig. 2. Tissue constructs labeled in the presence of 5% DMSO (Fig. 2b), 10% PVP (Fig. 2c) and 4% BSA (Fig. 2d) demonstrate labeling through a greater depth than those labeled in PBS only (Fig. 2a). For the corresponding anti-human IgG controls of the tissue constructs, some nonspecific labeling is seen with 10% PVP (Fig. 3a) and 4% BSA (Fig. 3b). The image shown in Fig. 3b for the 4% BSA IgG control showed the most fluorescence of all three trials, but it appears that the labeling is nonspecific when compared with the contrast agent in Fig. 2d, where individual cells can be clearly seen. The 10% PVP IgG control shown in Fig. 3a has a relative fluorescence intensity less than with the contrast agent shown in Fig. 2c. Fluorescence images of the same tissue constructs labeled in the presence of PBS and 5% DMSO obtained with a 40× objective are shown in Fig. 4. Cell membrane EGFR labeling of cells embedded in collagen is clearly evident in both cases, though labeling is more intense in the presence of 5% DMSO (Fig. 4c).

### Detection of EGFR in fresh tissue slices

Fluorescence images from a clinically abnormal and clinically normal biopsy pair are shown in Fig. 5a,b, labeled for EGFR using the contrast agent obtained with a 40× objective. Figure 5c,d shows the corresponding H&E images for the clinically abnormal and clinically normal biopsy, respectively. The abnormal biopsy was obtained from the retromolar trigone and diagnosed as moderate dysplasia of the squamous epithelium with underlying foci of invasive squamous carcinoma. The normal biopsy was obtained from the pharyngeal wall and diagnosed as normal with mild hyperkeratosis. The fluorescence intensity is considerably higher in the abnormal sample (Fig. 5a) than in the normal sample (Fig. 5b), by an average factor of 5×.

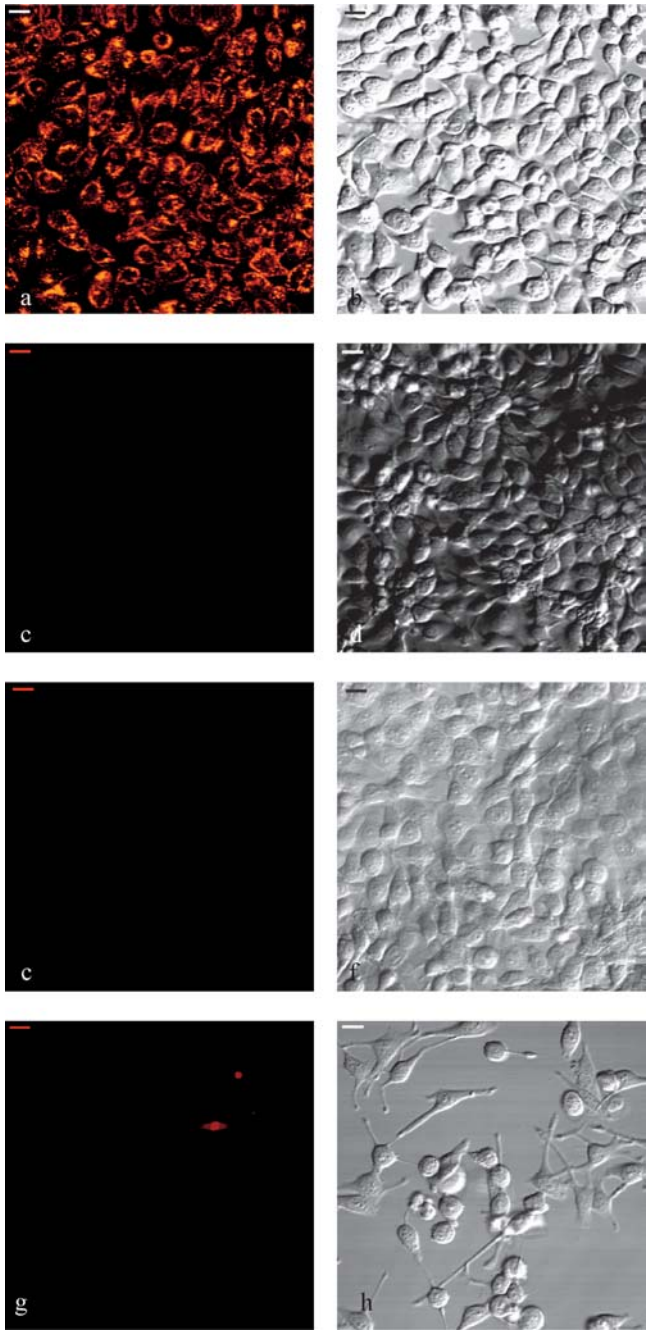


**Figure 1.** Confocal images of SqCC/Y1 and MDA-MB-435S cells taken with a 40× oil-immersion objective. False-color fluorescence images obtained at excitation 647 nm with a 665 nm long-pass filter (a,c,e,g). Transmitted DIC images (b,d,f,h). Scale bar in all images is 25μm. a: SqCC/Y1 cells labeled with anti-EGFR and Alexa Fluor® 660 streptavidin. b: Corresponding transmitted DIC image. c: SqCC/Y1 cells labeled with anti-human IgG and Alexa Fluor® 660 streptavidin. d: Corresponding transmitted DIC image. e: SqCC/Y1 cells labeled with Alexa Fluor® 660 streptavidin only, no antibody. f: Corresponding transmitted DIC image. g: MDA-MB-435S cells labeled with anti-EGFR and Alexa Fluor® 660 streptavidin. h: Corresponding transmitted DIC image.

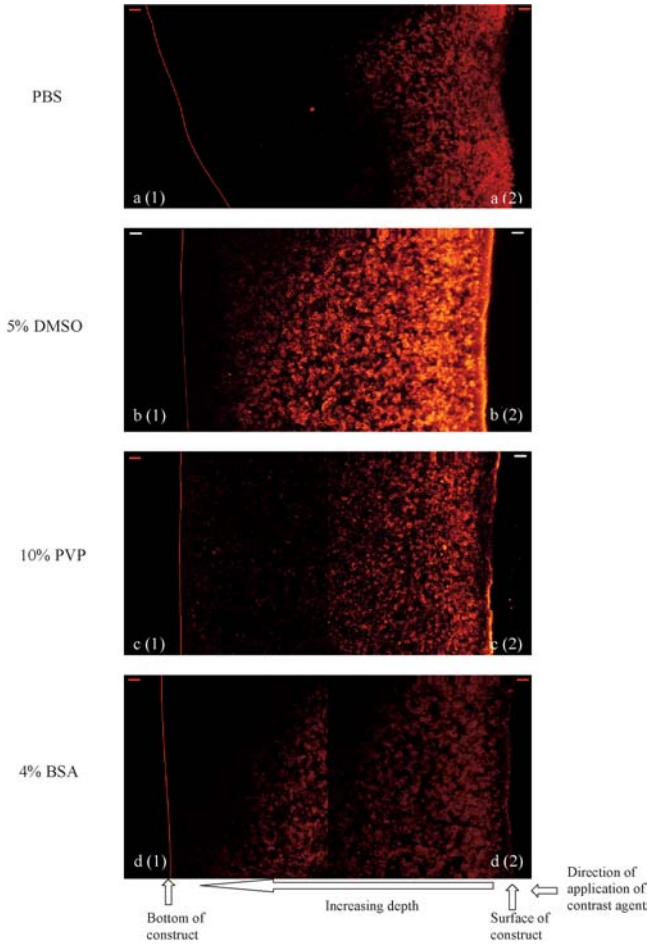


**Figure 2.** False-color confocal images of SqCC/Y1 tissue constructs labeled with anti-EGFR and Alexa Fluor® 660 streptavidin in the presence of permeability-enhancing agents taken with a 10× objective. The scale bar in all images is 100 μm. (2) Images are the top of the constructs with the contrast agent applied from the right. (1) Images are the bottom of the tissue construct, with the line representing the approximate location of the bottom of the construct. a: Tissue constructs labeled in the presence of PBS only. b: Tissue constructs labeled in the presence of 5% DMSO. c: Tissue constructs labeled in the presence of 10% PVP. d: Tissue constructs labeled in the presence of 4% BSA.

### Fluorometry of cells labeled for EGFR

The mean fluorescence intensities of SqCC/Y1 cells labeled for various incubation times and with various dilutions of EGFR antibody are shown in Fig. 6. In Fig. 6, the squares represent cells labeled for EGFR corrected for background intensity by subtracting IgG, and the diamonds represent cells labeled using the IgG control. Cells labeled for various incubation times of 5, 15, 30 and 60 min showed a linear increase in fluorescence with increasing incubation time as shown in Fig. 6a. Cells labeled using various dilutions of the EGFR antibody of 1:4, 1:10, 1:50 and 1:100 also showed a linear increase in fluorescence with increasing antibody concentration as shown in Fig. 6b. In both cases, the shortest incubation time and the lowest antibody dilution still demonstrated a significant increase in fluorescence compared with the control. Cells labeled in the presence of 0.0133 μ*M* EGF did not show a significant difference in fluorescence intensity compared with those labeled in the absence of EGF. However, the cells labeled in the presence of increasing concentrations of EGF showed a linear decrease in fluorescence intensity with increase in EGF concentration as shown in Fig. 7.

### Quantitative flow cytometry

The number of EGFR per cell was determined for SqCC/Y1 cells using the QIFI kit analysis. Approximately 300 000 receptors per

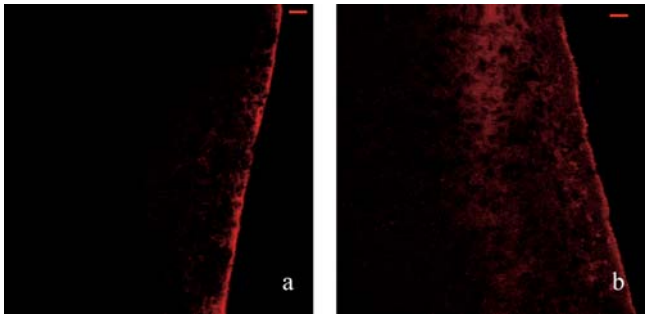


**Figure 3.** False-color confocal images of SqCC/Y1 tissue constructs labeled with anti-human IgG and Alexa Fluor® 660 streptavidin in the presence of permeability-enhancing agents taken with a 10× objective. The scale bar in both images is 100 μm. a: Tissue construct labeled in the presence of 10% PVP. b: Tissue construct labeled in the presence of 4% BSA.

cell were labeled (data not shown). Other investigators reported the number of EGFR per cell to be $4.70 \times 10^5$ to $8 \times 10^5$ (27,28), similar to that reported here.

### Cytotoxicity of Alexa Fluor® 660 streptavidin

The Alexa Fluor® 660 streptavidin had no effect on the viability of the cells after the 2 day incubation period. All samples had a viability of 98% or higher.

## DISCUSSION

*In vitro* experiments with cell cultures demonstrate that the contrast agent specifically targets the extracellular membrane of neoplastic cells and suggest specific targeting of EGFR. EGFR is a transmembrane protein; thus, as expected, fluorescence is seen primarily at the cell membrane, where the EGFR is located, and little to no fluorescence is seen with controls. The fluorometry competitive binding studies with EGF demonstrate that the contrast agent binds to a much lower degree in the presence of EGF, also suggesting that it is specifically targeting EGFR.

An advantage of using Alexa Fluor® 660 streptavidin is that it has a broad absorption peak, allowing it to be efficiently excited between 633 and 660 nm with emission at 690 nm. The broad excitation range allows the contrast agent to be used readily with the 633 nm laser line of a HeNe or the 647 nm laser line of a krypton ion laser while still maintaining a relatively long Stokes shift for easy rejection of elastically scattered excitation. An excitation wavelength greater than about 600 nm allows increased penetration depth into tissue with substantially reduced interference from autofluorescence of endogenous fluorophores and scattering and absorption from tissue structures.

Fluorometry experiments with varying dilutions of the EGFR antibody and varying incubation times indicate that the antibody can be used in relatively low concentrations and only short incubation times are required to achieve a detectable fluorescence signal. The use of low antibody concentrations is critical in the development of the contrast agent to minimize the possibility for immunogenic effects and to keep costs low. In addition, for clinical applications of the contrast agent, a short incubation time is critical to achieve expedient diagnosis with minimal patient discomfort and waiting time.

In this study, a 1:10 dilution of the EGFR antibody resulted in a concentration of 20 μg/mL, and the Alexa Fluor® 660 streptavidin dye was used at a concentration of 31.25 μg/mL. One hundred microliters of each, or 2 μg of the antibody and 3.1 μg of the dye, was used to label the multilayer tissue constructs, which consisted of approximately 32 million cells. A precancer with a 1 mm radius and 300 μm depth consists of approximately $10^6$ cells, so the amounts of antibody and dye used to label the multilayer tissue constructs are theoretically sufficient for detecting a precancerous lesion. Cetuximab is an EGFR antibody produced by ImClone Systems (Somerville, NJ), which is currently in clinical trials for treatment of several types of solid tumors, including head and neck. The current recommended dosage is an initial loading dose of 400 mg/m$^2$ and maintenance dose of 200 mg/m$^2$ (29). The body surface area of an individual using the average height and weight statistics given by the Centers for Disease Control and Prevention (CDC) is 2 m$^2$, resulting in a Cetuximab loading dose of 800 mg and maintenance dose of 400 mg. Drug dosage is difficult to directly compare to the amounts of antibody used in this study because the goal of the Cetuximab treatment is cancer therapy rather than diagnosis and dosage is given in terms of body surface area, but it is clear that the amounts of EGFR antibody required for diagnostic imaging are considerably less than the amounts administered for therapeutic reasons with tolerable side effects. Although the number of cells in the multilayer tissue construct cannot be extrapolated directly to the number of cells in an *in vivo* solid tumor, these numbers indicate that the concentrations of antibody and dye being used here are not unreasonable for clinical use.

Numerous studies have achieved localization of target-specific near-infrared fluorescent contrast agents to tumors using monoclonal antibodies or peptide delivery platforms *in vivo* in animal models (24,30–33); however, in all cases, the conjugate was

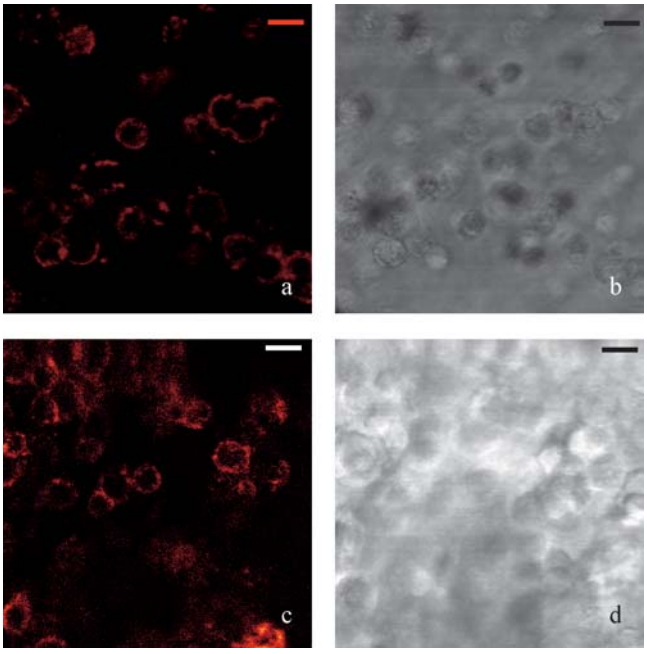


**Figure 4.** Confocal images of SqCC/Y1 tissue constructs labeled with anti-EGFR and Alexa Fluor® 660 streptavidin taken with a 40× oil-immersion objective. False-color fluorescence images obtained at excitation 647 nm with a 665 nm long-pass filter (a,c). Transmitted DIC images (b,d). Scale bar in all images is 25 μm. Tissue constructs labeled in the presence of PBS only (a,b). Tissue constructs labeled in the presence of 5% DMSO (c,d).

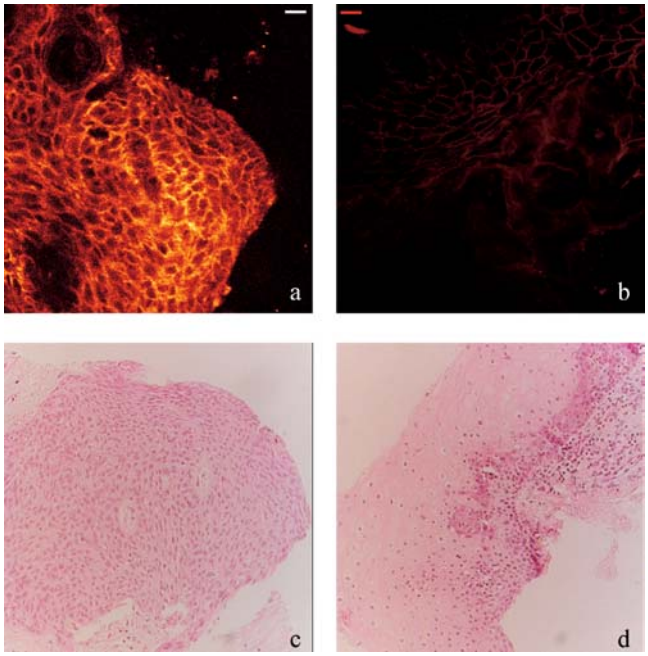


**Figure 5.** Confocal images of tissue slices from a (a) clinically abnormal and (b) clinically normal biopsy pair and corresponding H&E images (c and d, respectively). Confocal images taken with a 40× oil-immersion objective; scale bar is 25 μm. H&E images taken with a 10× objective. Abnormal biopsy taken from the retromolar trigone. Diagnosis of (c) was moderate dysplasia in the epithelium with foci of moderately differentiated cancer. Normal biopsy taken from the pharyngeal wall. Diagnosis of (d) was normal with mild hyperkeratosis.

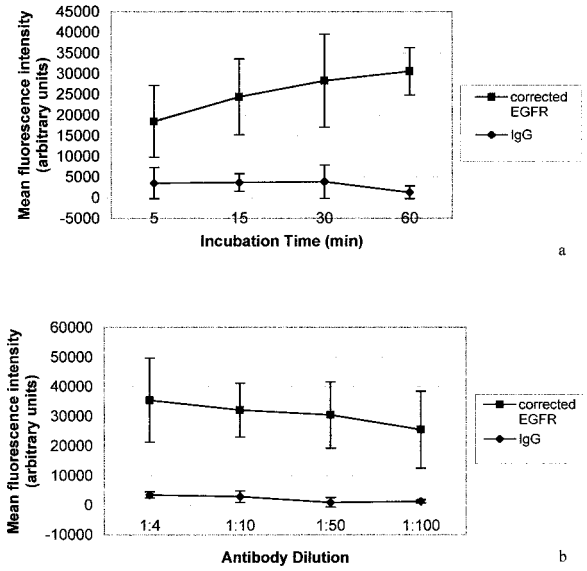


**Figure 6.** a: Fluorescence intensities for SqCC/Y1 cells labeled for various incubation times using a 1:10 antibody dilution averaged over three trials. b: Fluorescence intensities for SqCC/Y1 cells labeled with different dilutions of antibody using a 60 min incubation time averaged over three trials. In both graphs, the PBS background and background produced by the supernatant of the cell suspension have been corrected in all samples. The squares represent cells labeled using EGFR, corrected for the background intensity of cells by subtracting the IgG sample. The diamonds represent cells labeled using the IgG control.

delivered via i.v. or intraperitoneal injection. In contrast, we are exploring methods to achieve labeling through topical application of the contrast agent. Topical application of the contrast agent is ideal to reduce systemic exposure to the contrast agent and to minimize the discomfort associated with i.v. injection. However, to label deeper lesions through topical application, the contrast agent may have to be applied in conjunction with permeability-enhancing agents to increase the penetration depth through multiple layers of epithelial cells. DMSO, PVP and BSA have all been applied as penetration enhancers across biomembranes, cell monolayers and multiple layers of epithelial cells (34–38). All three permeability-enhancing agents tested here, 5% DMSO, 10% PVP and 4% BSA, increased penetration of the contrast agent relative to PBS in tissue constructs. Tissue constructs labeled in the presence of either DMSO or PVP demonstrated fluorescence to the bottom of the tissue construct, approximately 500 μm.

The ability to distinguish abnormal from normal tissue based on fluorescence intensity of the contrast agent was achieved. In the biopsy pair presented here, the dysplastic slice had a fluorescence intensity five times greater than that of the normal slice. Histologically, the abnormal slice contained both dysplasia in the epithelium and foci of moderately differentiated cancer, whereas the normal slice was normal with mild hyperkeratosis. Although EGFR is expressed in normal tissue, the likelihood is that overexpression of EGFR in abnormal tissue provides sufficiently increased fluorescence intensity to discriminate abnormal from normal tissue. In addition, although the elevation of EGFR in normal-early hyperplasia and in normal tissue adjacent to tumor may lead to false-positive diagnoses, it also has the possibility to facilitate early detection by providing a marker for tissue that is likely to undergo carcinogenesis and should be monitored. A preliminary clinical study testing at least 20 pairs of abnormal and normal biopsies from the oral cavity is currently in progress to determine the efficacy of distinguishing abnormal from normal tissue based on the fluorescence intensity of the contrast agent.

Fluorescence spectroscopy or imaging (or both) could be used to detect the signal of the contrast agent *in vivo* and localize potential tumors or tumor margins. In addition, with the development of fiber-based *in vivo* confocal microscopes (39–44), including the commercially available fiber-based confocal fluorescence microscopes produced by OptiScan Imaging Limited (Melbourne, Victoria, Australia) and Mauna Kea Technologies (Paris, France), the contrast agent could be used to provide additional signal for imaging applications to the epithelial layer *in vivo* to allow for diagnosis of abnormal tissue.

With respect to *in vivo* use of the contrast agent, questions concerning the use of the biotin–(strept)avidin system and the various permeability-enhancing agents must be addressed. The high-affinity biotin–(strept)avidin system has been used *in vivo* in radioapplications, including radioimmunodetection and therapy of cancer in humans (45) and immunotargeting of cytotoxic molecules and cells to tumor cells (37,46–49). The possible drawbacks in using streptavidin for *in vivo* applications are that it tends to be sequestered quickly by the kidneys (50), which could limit the amount of the streptavidin-conjugated compound delivered to the target, and it cannot be humanized, potentially making it more immunogenic. Streptavidin has been modified to improve its *in vivo* sequestration characteristics (50); however, kidney localization of the streptavidin-labeled dye before tumor targeting is not likely to be a problem with topical application of the contrast agent. Further, streptavidin is an analog of avidin,

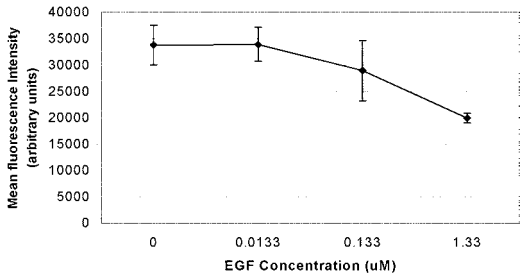


**Figure 7.** Fluorescence intensities for SqCC/Y1 cells labeled with the contrast agent in the absence of EGF and in the presence of 0.0133, 0.133 and 1.33 μ*M* EGF averaged over three trials. All samples are corrected for the PBS background and background produced by the supernatant of the cell suspension.

which has better immunogenic characteristics but a much shorter circulatory half-life (45) and could replace streptavidin in the contrast agent for biotin binding.

The presence of endogenous biotin could result in false-positive staining because of endogenous avidin-binding activity (EABA); however, studies that investigated the levels of background EABA in tissue sections from various organ sites found levels to be high only in tissues known to contain large biotin stores, which include liver, adipose tissue, mammary gland and kidney (51). We are therefore hopeful that in the oral cavity, EABA levels will be low and not contribute significant background.

Clinically, DMSO has been approved by the Food and Drug Administration (FDA) for use in treatment of interstitial cystitis and is delivered as a 50% solution or in a DMSO cocktail, which contains 50 cc of 50% DMSO (52). According to FDA toxicological data for Class-3 solvents, the permitted daily exposure of DMSO is 50 mg/day or approximately 500 mol/day. Five-hundred microliters of a 5% solution of DMSO contains only 0.35 mmol of DMSO. In addition, PVP has been approved by the FDA as an excipient in topical formulations and is used in a povidone–iodine solution, ranging from 1% to 20% in drugs from various pharmaceutical companies (information from the FDA Center for Drug Evaluation and Research website).

A number of significant issues must be addressed before performing clinical trials with this contrast agent. Although initial studies are encouraging for the lack of cytotoxic effects of the dye, longer-term toxicity studies need to be performed both in cell and animal models. In addition, other issues that must be considered are possible immunogenic effects of the antibody, optimal time for localization of the contrast agent to neoplasia and subsequent imaging and clearance of the contrast agent from the tissues. Although these pharmacokinetic issues will need to be addressed, we have demonstrated that the contrast agent has the ability to target EGFR-positive cells in viable *in vitro* biological models of cell monolayers and cell suspensions, that deeper labeling is possible through topical application and the use of permeability-enhancing agents and that there is the potential to distinguish abnormal from normal tissue based on fluorescence intensity in *ex vivo* biopsy samples.

*Acknowledgements*—Quantitative flow cytometry was performed by Kent Claypool at the University of Texas M.D. Anderson Cancer Center Science Park Research Division. Funding was provided by National Science Foundation (NSF) grant BES-0086736, NIH grant R21EB002165, and NSF grant DGE-9870653. We thank Vivian Mack and Saima Ghori for assistance with tissue culture work.

## REFERENCES

1. Andersson-Engels, S., C. a. Klinteberg, K. Svanber and S. Svanber (1997) *In vivo* fluorescence imaging for tissue diagnostics. *Phys. Med. Biol.* **42**, 815–824.
2. Ferris, D. G., R. A. Lawhead, E. D. Dickman, N. Holtzapple, J. A. Miller, S. Grogan, S. Bambot, A. Agrawal and M. L. Faupel (2001) Multimodal hyperspectral imaging for the noninvasive diagnosis of cervical neoplasia. *J. Low. Genital Tract Dis.* **5**(2), 65–72.
3. Gurjar, R. S., V. Backman, L. T. Perelman, I. Georgakoudi, K. Badizadegan, I. Itzkan, R. R. Dasari and M. S. Feld (2001) Imaging human epithelial properties with polarized light-scattering spectroscopy. *Nat. Med.* **7**(11), 1245–1248.
4. Collier, T., A. Lacy, R. Richards-Kortum, A. Malpica and M. Follen (2002) Near real-time confocal microscopy of amelanotic tissue: detection of dysplasia in *ex vivo* cervical tissue. *Acad. Radiol.* **9**, 504–512.
5. White, W. M., M. Rajadhyaksha, S. Gonzalez, R. L. Fabian and R. R. Anderson (1999) Noninvasive imaging of human oral mucosa *in vivo* by confocal reflectance microscopy. *Laryngoscope* **109**, 1709–1717.
6. Sokolov, K., R. Drezek, K. Gossage and R. Richards-Kortum (1999) Reflectance spectroscopy with polarized light: is it sensitive to cellular and nuclear morphology? *Opt. Express* **5**(13), 302.
7. Sokolov, K., M. Follen and R. Richards-Kortum (2002) Optical spectroscopy for detection of neoplasia. *Curr. Opin. Chem. Biol.* **6**, 651–658.
8. Utzinger, U., M. Brewer, E. Silva, D. Gersheson, R. C. Blast, Jr., M. Follen and R. Richards-Kortum (2001) Reflectance spectroscopy for *in vivo* characterization of ovarian tissue. *Lasers Surg. Med.* **28**, 56–66.
9. Gillenwater, A., R. Jacob and R. Richards-Kortum (1998) Fluorescence spectroscopy: a technique with potential to improve the early detection of aerodigestive tract neoplasia. *Head Neck* **20**, 556–562.
10. Ramanujam, N. (2000) Fluorescence spectroscopy of neoplastic and non-neoplastic tissues. *Neoplasia* **2**(1–2), 89–117.
11. Wagnières, G. A., W. M. Star and B. C. Wilson (1998) *In vivo* fluorescence spectroscopy and imaging for oncological applications. *Photochem. Photobiol.* **68**(5), 603–632.
12. Müller, M. G., T. A. Valdez, I. Georgakoudi, V. Backman, C. Fuentes, S. Kabani, N. Laver, Z. Wang, C. W. Boone, R. R. Dasari, S. M. Shapshay and M. S. Feld (2003) Spectroscopic detection and evaluation of morphologic and biochemical changes in early human oral carcinoma. *Cancer* **97**(7), 1681–1692.
13. Svistun, E., R. Alizadeh-Naderi, A. El-Naggar, R. Jacob, A. Gillenwater and R. Richards-Kortum (2003) Vision enhancement system for detection of oral cavity neoplasia based on autofluorescence. *Head Neck* 205–215.
14. Schantz, S. P., V. Kolli, H. E. Savage, G. Yu, J. P. Shah, D. E. Harris, A. Katz, R. R. Alfano and A. G. Huvos (1998) *In vivo* native cellular fluorescence and histological characteristics of head and neck cancers. *Clin. Cancer Res.* **4**, 1177–1182.
15. Betz, C. S., M. Mehlmann, K. Rick, H. Stepp, G. Grevers, R. Baumgartner and A. Leunig (1999) Autofluorescence imaging and spectroscopy of normal and malignant mucosa in patients with head and neck cancer. *Lasers Surg. Med.* **25**, 323–334.
16. Heintzelman, D. L., U. Utzinger, H. Fuchs, A. Zuluaga, K. Gossage, A. M. Gillenwater, R. Jacob, B. Kemp and R. R. Richards-Kortum (2000) Optimal excitation wavelengths for *in vivo* detection of oral neoplasia using fluorescence spectroscopy. *Photochem. Photobiol.* **72**(1), 103–113.
17. Srinivas, P. R., B. S. Kramer and S. Srivastava (2001) Trends in biomarker research for cancer detection. *Lancet Oncol.* **2**, 698–704.
18. Kannan, S., P. Balaram, G. J. Chandran, M. R. Pillai, B. Mathew and M. K. Nair (1994) Co-expression of ras p21 and epidermal growth factor receptor during various stages of tumour progression in oral mucosa. *Tumor Biol.* **15**, 73–81.
19. Shintani, S., T. Matsumura, R. E. Alcalde and Y. Yoshihama (1996) Sequential expression of *myc-, ras-*, oncogene products and EGF receptor during DMBA-induced tongue carcinogenesis. *Int. J. Oncol.* **8**, 821–826.
20. Shin, D. M., J. Y. Ro, W. K. Hong and W. N. Hittelman (1994) Dysregulation of epidermal growth factor receptor expression in premalignant lesions during head and neck tumorigenesis. *Cancer Res.* **54**, 3153–3159.

21. van Oijen, M. G. C. T., G. Rijksen, F. W. ten Broek and P. J. Slootweg (1998) Increased expression of epidermal growth factor receptor in normal epithelium adjacent to head and neck carcinomas independent of tobacco and alcohol abuse. *Oral Dis.* **4**, 4–8.
22. Nouri, A. M. E., C. Thompson, H. Cannell, M. Symes, S. Purkiss and Z. Amirghofran (2000) Profile of epidermal growth factor receptor (EGFr) expression in human malignancies: effects of exposure to EGF and its biological influence on established human tumour cell lines. *Int. J. Mol. Med.* **6**, 495–500.
23. Todd, R. and D. T. W. Wong (1999) Epidermal growth factor receptor (EGFR) biology and human oral cancer. *Histol. Histopathol.* **14**, 491–500.
24. Soukos, N. S., M. R. Hamblin, S. Keel, R. L. Fabian, T. F. Deutsch and T. Hasan (2001) Epidermal growth factor receptor-targeted immunophotodiagnosis and photoimmunotherapy of oral precancer *in vivo*. *Cancer Res.* **61**, 4490–4496.
25. Sokolov, K., J. Galvan, A. Myakov, A. Lacy, R. Lotan and R. Ricards-Kortum (2002) Realistic three-dimensional epithelial tissue phantoms for biomedical optics. *J. Biomed. Opt.* **71**(1), 148–156.
26. Anido, J., P. Matar, J. Albanell, M. Guzmán, F. Rojo, J. Arribas, S. Averbuch and J. Baselga (2003) ZD1839, a specific epidermal growth factor receptor (EGFR) tyrosine kinase inhibitor, induces the formation of inactive EGFR/HER2 and EGFR/HER3 heterodimers and prevents heregulin signaling in HER2-overexpression breast cancer cells. *Clin. Cancer Res.* **9**, 1274–1283.
27. King, I. and A. C. Sartorelli (1989) Epidermal growth factor receptor gene expression, protein kinase activity, and terminal differentiation of human malignant epidermal cells. *Cancer Res.* **49**(20), 5677–5681.
28. Reiss, M., E. B. Stash, V. F. Vellucci and Z.-L. Zhou (1991) Activation of the autocrine transforming growth factor $\alpha$ pathway in human squamous carcinoma cells. *Cancer Res.* **51**(23 Pt 1), 6254–6262.
29. Baselga, J. (2001) The EGFR as a target for anticancer therapy—focus on cetuximab. *Eur. J. Cancer* **37**, S16–S22.
30. Becker, A., C. Hessenius, K. Licha, B. Ebert, U. Sukowski, W. Semmier, B. Wiedenmann and C. Grötzinger (2001) Receptor-targeted optical imaging of tumors with near-infrared fluorescent ligands. *Nat. Biotechnol.* **19**, 327–331.
31. Bugaj, J. E., S. Achilefu, R. B. Dorshow and R. Rajagopalan (2001) Novel fluorescent contrast agents for optical imaging of *in vivo* tumors based on a receptor-targeted dye-peptide conjugate platform. *J. Biomed. Opt.* **6**(2), 122–133.
32. Sevick-Muraca, E. M., J. P. Houston and M. Gurfinkel (2002) Fluorescence-enhanced, near infrared diagnostic imaging with contrast agents. *Curr. Opin. Chem. Biol.* **6**, 642–650.
33. Ballou, B., G. W. Fisher, T. R. Hakala and D. L. Farkas (1997) Tumor detection and visualization using cyanine fluorochrome-labeled antibodies. *Biotechnol. Prog.* **13**, 649–658.
34. Krishna, G., K.-J. Chen, C.-C. Lin and A. A. Nomeir (2001) Permeability of lipophilic compounds in drug discovery using *in-vitro* human absorption model, caco-2. *Int. J. Pharm.* **222**, 77–89.
35. Viegas, T. X., A. H. Hikal and R. W. Cleary (1998) Formulation of penetration enhancers in polymers. *Drug Dev. Ind. Pharm.* **14**(6), 855–866.
36. Yu, Z.-W. and P. J. Quinn (1995) Dimethyl sulphoxide: a review of its applications in cell biology. *Biosci. Rep.* **14**(6), 259–281.
37. Yu, Z.-W. and P. J. Quinn (1998) The modulation of membrane structure and stability by dimethyl sulphoxide. *Mol. Membr. Biol.* **15**, 59–68.
38. Sokolov, K., M. Follen, J. Aaron, I. Pavlova, A. Malpica, R. Lotan and R. Richards-Kortum (2003) Real time vital optical imaging of precancer using anti-EGF receptor antibodies conjugated to gold nanoparticles. *Cancer Res.* **63**(9), 1999–2004.
39. Sung, K. B., C. Liang, M. Descour, T. Collier, M. Follen, A. Malpica and R. Richards-Kortum (2002) Near real time *in vivo* fibre optic confocal microscopy: sub-cellular structure resolved. *J. Microsc.* **207**(Pt 2), 137–145.
40. Sung, K. B., C. Liang, M. Descour, M. Follen and R. Richards-Kortum (2002) Fiber optic confocal microscope with miniature objective for *in-vivo* imaging. *IEEE Trans. Biomed. Eng.* **49**(10), 1168–1172.
41. Anikijenko, P., L. T. Vo, E. R. Murr, J. Carrasco, W. J. McLaren, Q. Chen, S. G. Thomas, P. M. Delaney and R. G. King (2001) *In vivo* detection of small subsurface melanomas in athymic mice using noninvasive fiber optic confocal imaging. *J. Investig. Dermatol.* **117**, 1442–1448.
42. Gmitro, A. F. and D. Aziz (1993) Confocal microscopy through a fiber-optic imaging bundle. *Opt. Lett.* **18**(8), 565–567.
43. Juškaitis, R. and T. Wilson (1992) Imaging in reciprocal fibre-optic based confocal scanning microscopes. *Opt. Commun.* **92**, 315–325.
44. Swindle, L. D., S. G. Thomas, M. Freeman and P. M. Delaney (2003) View of normal human skin *in vivo* as observed using fluorescent fiber-optic confocal microscopic imaging. *J. Investig. Dermatol.* **121**, 706–712.
45. Boerman, O. C., F. G. van Schaijk, W. J. G. Oyen and F. H. M. Corstens (2003) Pretargeted radioimmunotherapy of cancer: progress step by step. *J. Nucl. Med.* **44**(3), 400–411.
46. Moro, M., M. Pelagi, G. Fulci, G. Paganelli, P. Dellabona, G. Casorati, A. G. Siccardi and A. Corti (1997) Tumor cell targeting with antibody-avidin complexes and biotinylated tumor necrosis factor $\alpha$. *Cancer Res.* **57**, 1922–1928.
47. Reali, E., J. W. Greiner, A. Corti, H. J. Gould, F. Bottazzoli, G. Paganelli, J. Schlom and A. G. Siccardi (2001) IgEs targeted on tumor cells: therapeutic activity and potential in the design of tumor vaccines. *Cancer Res.* **61**, 5517–5522.
48. Schechter, B., R. Arnon, M. Wilchek, J. Schlessinger, E. Hurwitz, E. Aboud-Pirak and M. Sela (1991) Indirect immunotargeting of Cis-Pt to human epidermoid carcinoma KB using the avidin-biotin system. *Int. J. Cancer* **48**, 167–172.
49. Guttinger, M., F. Guidi, M. Chinol, E. Reali, F. Veglia, G. Viale, G. Paganelli, A. Corti and A. G. Siccardi (2000) Adoptive immunotherapy by avidin-driven cytotoxic T lymphocyte tumor bridging. *Cancer Res.* **60**, 4211–4215.
50. Wilbur, D. S., P. M. Pathare, D. K. Hamlin, P. S. Stayton, R. To, L. A. Klumb, K. R. Buhler and R. L. Vessella (1999) Development of new biotin/streptavidin reagents for pretargeting. *Biomol. Eng.* **16**, 113–118.
51. Wood, G. S. and R. Warnke (1981) Suppression of endogenous avidin-binding activity in tissues and its relevance to biotin-avidin detection systems. *J. Histochem. Cytochem.* **29**(10), 1196–1204.
52. Moldwin, R. M. and G. R. Sant (2002) Interstitial cystitis: a pathophysiology and treatment update. *Clin. Obstet. Gynecol.* **45**, 259–272.